Long-wave linear stability theory for two-fluid channel flow

Tetyana M. Segin[(1)], **Lou Kondic**[(2)], **Burt S. Tilley**[(3)]

[(1)] Department of Chemical and Materials Engineering

University of Alberta, Edmonton, Alberta, Canada T6G 2G6

[(2)] Department of Mathematical Sciences and

Center for Applied Mathematics and Statistics

New Jersey Institute of Technology, Newark, NJ 07102

[(3)] Franklin W. Olin College of Engineering

Needham, MA 02492

CAMS Report 0405-30, Spring 2005

Center for Applied Mathematics and Statistics

NJIT

Long-wave linear stability theory for two-fluid channel flow including compressibility effects

Tetyana M. Segin

Department of Chemical and Materials Engineering

University of Alberta, Edmonton, Alberta, Canada T6G 2G6

Lou Kondic

Department of Mathematical Sciences

Center for Applied Mathematics and Statistics

New Jersey Institute of Technology

Newark, NJ 07102

Burt S. Tilley

Franklin W. Olin College of Engineering

Needham, MA 02492

(Dated: May 19, 2005)

We present the linear stability of the laminar flow of an immiscible system of a compressible gas and incompressible liquid separated by an interface with large surface tension in a thin inclined channel. The flow is driven by an applied pressure drop and gravity. Following the air-water case, which is found in a variety of engineering systems, the ratio of the characteristic values of the gas and liquid densities and viscosities are assumed to be disparate. Under lubrication approximation, and assuming ideal gas behavior and isothermal conditions, this approach leads to a coupled nonlinear system of partial differential equations describing the evolution of the interface between the gas and the liquid and the streamwise density distribution of the gas. This system also includes the effects of viscosity stratification, inertia, shear, and capillarity. A linear stability analysis that allows for physically relevant nonzero

pressure-drop base state is then performed. In contrast to zero-pressure drop case which is amenable to the classical normal-mode approach, this configuration requires solving numerically a nonautonomous boundary-value problem for the gas density and interfacial deviations from the base state in the streamwise coordinate. We find that the effect of gas compressibility on the interfacial stability in the limit of vanishingly small wavenumber is destabilizing, even for Stokes flow in the liquid. However, for finite wavenumber disturbances, compressibility may have stabilizing effects. In this regime, sufficient shear is required to destabilize the flow.

I. INTRODUCTION

Liquid films are encountered in many physical situations. Examples of their practical application include oil and gas flows (see Oddie and Pearson [15] for recent review), variety of cooling applications (see, e.g., Mudawar [14], Qu and Mudawar [17]), in particular related to on-chip cooling of micro-electromechanical (MEMS) devices (Pettigrew, Kirshberg, Yerkes, Trebotich and Liepmann [16], Trebotich, Kirshberg, Teng and Liepmann [24], Kirshberg, Yerkes, Liepmann and Trebotich [11]). Two-phase gas-liquid flows are also important in a number of space operations including the design and operation of spacecraft environmental systems (Zhang [26]), storage and transfer of cryogenic fluids and safety and performance issues related to space nuclear power systems (Dukler and Smith [7], Bousman, McQuillen and Witte [4]). Knowledge about the physical properties of fluids and their effects on flow characteristics is important to understand the fundamental nature of two-phase flow.

Most of the existing theoretical works on two-fluid flows neglect compressibility of both fluids, even if one of them is a gas. Often, this approximation is motivated by the fact that Mach number may be small in these flows. However, compressibility *cannot* be neglected in flows gases through narrow channels even if Mach number is small (Faber [8]). In these flows, an appreciable pressure difference may exist between the inlet and outlet regions,

resulting in appreciable density changes. This effect is particularly relevant for flows in microchannels [14, 17].

There are several works devoted to weakly compressible flows. In this limit, Hagstrom and Lorenz [10] find that the solution remains smooth for all times and, to leading order, it consists of the corresponding incompressible flow plus a highly oscillatory part describing sound waves. Alexakis, Young and Rosner [1], motivated by an astrophysical problem (where mixing across material interfaces driven by shear flows may significantly affect the dynamical evolution) show in their linear stability analysis that compressibility decreases the growth rate of instability. Rusak and Lee [18] investigate the influence of the compressibility on the appearance of instabilities and transition (breakdown) phenomena in a compressible inviscid axisymmetric and rotating columnar flow of perfect gas in a finite-length straight circular pipe. They report the stabilizing effect of compressibility on vortex flows. The results are not so clear in the flows that are subject to Rayleigh-Taylor instability, where compressibility can have both stabilizing and destabilizing effects; see Livescu [12] and the references therein.

Figure 1 shows the basic geometry of the flow considered in this work. The two fluids can flow either cocurrently (both fluids flow in the same direction) or countercurrently (fluids flow in the opposite directions). Various aspects of the transition from the countercurrent flow (shown in Fig. 1) to a cocurrent flow adverse to gravity, as the adverse pressure drop is increased is called *flooding*. Flooding has been investigated extensively both phenomenologically (Chang [5], Fowler and Lisseter [9]) and experimentally (see Bankoff and Lee [2] and the references therein, Mouza, Paras and Karabelas [13]) but the criteria for onset of flooding and related interfacial instabilities is still an open question. The main goal of the present paper is to explore the interfacial stability in two-fluid channel flow, in particular regarding the influence of compressibility. We mostly concentrate on countercurrent flow, which is of particular interest to the applications involving flooding.

The paper is organized as follows. In Section II we derive equations that govern the interfacial dynamics for the flow of incompressible liquid and compressible gas. Section III

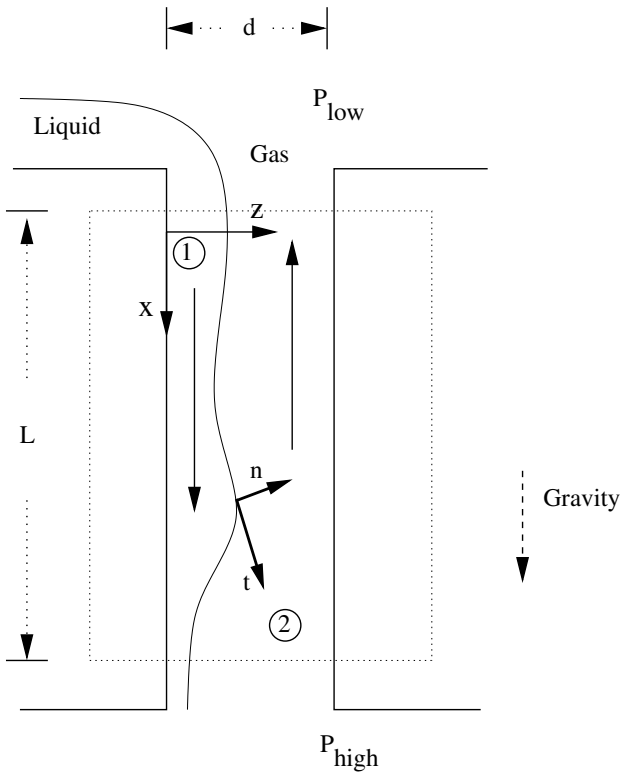

FIG. 1: Basic outline of the problem of interest. The plate on the left is coated by a liquid driven by gravity (pointing down), while the gas is driven by an adverse pressure drop (higher pressure at the bottom). This system can undergo hydrodynamic instabilities for sufficiently large adverse pressure drops. We consider only the domain in the dashed box in this work, and do not include the entrance or exit effects in the liquid or the gas. The local coordinate frame, based on the channel, is also shown.

is devoted to the linear stability analysis. For reference, we consider incompressible limit in Section 3.1, and then concentrate on compressible case. Here, we observe that the general boundary condition for the density equation (prescribed values of the gas density at each end of the channel) imply that in general the basic density state depends on the downstream coordinate. A simpler case where this dependence is absent is considered in Section 3.2. In this case, we proceed with the normal mode analysis to investigate the behavior of both interfacial and density modes. In Section 3.3, we consider the dynamics of countercurrent two-fluid flow for the case when the prescribed density values are different, and the base

state is space dependent. In Section 4 we discuss the effect of compressibility on the interface stability in all considered configurations.

II. FORMULATION OF EQUATIONS

Consider the flow of two viscous fluids in a channel of height d and length L (Figure 1) under isothermal conditions, where $\mathbf{n}$ is the unit normal pointing from the incompressible phase 1 (liquid) into the compressible phase 2 (gas), and $\mathbf{t}$ is the unit tangent vector at the interface. The equations that govern this system are continuity, the Navier-Stokes equations, and a equation of state for the gas (asterisks denote dimensional variables):

$$\begin{aligned}
\bar{\nabla} \cdot \mathbf{u}^{*(1)} &= 0, \\
\rho_1^* \left(\frac{\partial \mathbf{u}^{*(1)}}{\partial t^*} + \mathbf{u}^{*(1)} \cdot \bar{\nabla} \mathbf{u}^{*(1)} \right) &= -\bar{\nabla} p^{*(1)} + \rho_1^* \mathbf{g} + \mu_1^* \bar{\nabla}^2 \mathbf{u}^{*(1)}, \\
\rho_{2t^*}^* + \bar{\nabla} \cdot (\rho_2^* \mathbf{u}^{*(2)}) &= 0, \\
\rho_2^* \left(\frac{\partial \mathbf{u}^{*(2)}}{\partial t^*} + \mathbf{u}^{*(2)} \cdot \bar{\nabla} \mathbf{u}^{*(2)} \right) &= -\bar{\nabla} p^{*(2)} + \rho_2^* \mathbf{g} + \mu_2^* \left(\bar{\nabla}^2 \mathbf{u}^{*(2)} + \frac{1}{3} \bar{\nabla} (\bar{\nabla} \cdot \mathbf{u}^{*(2)}) \right), \\
p^{*(2)} &= K^* \rho_2^*.
\end{aligned}$$

The superscripts (1) and (2) on the dependent velocity and pressure variables correspond to phase 1 and phase 2, respectively, with corresponding densities ρ_i^*, dynamical viscosities μ_i^* and pressures $p^{*(i)}$; $\mathbf{g}$ is the gravitational acceleration. The last equation in the system relates the pressure and the density of the ideal gas under isothermal conditions ($pV = nRT$). $K^* = RT^*/M$, where R is the universal gas constant, T^* is the ambient temperature, and M is the molecular weight of the gas, which gives that $\rho_2^* = nM/V$, where n is the number of moles of gas in the layer and V is the volume of the gas. Note further that in this case K^* also represents the square of the speed of sound in the gas layer.

The velocities $\mathbf{u}^{*(i)} = (u^{*(i)}, w^{*(i)})$ satisfy the usual no-slip and no-penetration boundary conditions on the channel walls: $\mathbf{u}^{*(1)} = 0$ on z^*=0 and $\mathbf{u}^{*(2)} = 0$ on $z^* = d$, as well as the balance of normal stress, balance of tangential stress, continuity of normal and tangential

components of velocity and kinematic condition at $z^* = h^*(x^*, t^*)$:

$$[\mathbf{n} \cdot \mathbf{T}^* \cdot \mathbf{n}] = \sigma^* \kappa^*, \tag{1}$$

$$[\mathbf{t} \cdot \mathbf{T}^* \cdot \mathbf{n}] = 0, \tag{2}$$

$$[\mathbf{u}^* \cdot \mathbf{n}] = 0, \tag{3}$$

$$[\mathbf{u}^* \cdot \mathbf{t}] = 0, \tag{4}$$

$$h^*_{t^*} + u^* h^*_{x^*} - w^* = 0, \tag{5}$$

where the jump $[f]$ of the quantity f across the interface is denoted by $[f] = f^{(2)} - f^{(1)}$; $\mathbf{T}^*$ denotes the stress tensor, σ^* is the surface tension between the two fluids, and κ^* is twice the mean curvature of the interface, given by

$$\kappa^* = -h^*_{x^* x^*} \left(1 + h^{*2}_{x^*}\right)^{-3/2}.$$

We scale lengths by d, densities by ρ_1^*, and velocities by $d^2 g/\nu_1^*$ ($\nu_1^* = \mu_1^*/\rho_1^*$ is the kinematic viscosity of phase 1) and

$$t = t^* dg/\nu_1^*, \tag{6}$$

$$p^{(i)} = p^{*(i)}/\rho_1^* dg. \tag{7}$$

Thus, we obtain

$$\nabla \cdot \mathbf{u}^{(1)} = 0, \tag{8}$$

$$Re_l \left\{ \frac{\partial \mathbf{u}^{(1)}}{\partial t} + \mathbf{u}^{(1)} \cdot \nabla \mathbf{u}^{(1)} \right\} = -\nabla p^{(1)} + \hat{\mathbf{g}} + \nabla^2 \mathbf{u}^{(1)}, \tag{9}$$

$$\bar{\rho}_t + \nabla \cdot (\bar{\rho} \mathbf{u}^{(2)}) = 0, \tag{10}$$

$$Re_l \bar{\rho} \left\{ \frac{\partial \mathbf{u}^{(2)}}{\partial t} + \mathbf{u}^{(2)} \cdot \nabla \mathbf{u}^{(2)} \right\}$$
$$= -\nabla p^{(2)} + \bar{\rho} \hat{\mathbf{g}} + \bar{\mu} \left\{ \nabla^2 \mathbf{u}^{(2)} + \frac{1}{3} \nabla \left[\nabla \cdot \mathbf{u}^{(2)} \right] \right\}, \tag{11}$$

$$p^{(2)} = K \bar{\rho}, \tag{12}$$

where $\bar{\rho} = \rho_2^*/\rho_1^*$ is the density ratio, $\bar{\mu} = \mu_2^*/\mu_1^*$ is the viscosity ratio, $K = K^*/dg$, $Re_l = gd^3/\nu_1^{*2}$ is the Reynolds number of phase 1, $\hat{\mathbf{g}}$ is the unit vector in the direction of gravity, and velocities are $\mathbf{u}^{(i)} = (u^{(i)}, w^{(i)})$.

The boundary conditions on the channel walls become: $\mathbf{u}^{(1)} = 0$ on z=0 and $\mathbf{u}^{(2)} = 0$ on $z = 1$ (Figure 1). The conditions (1) - (5) at $z = h(x,t)$ become

$$[\mathbf{n} \cdot \mathbf{T} \cdot \mathbf{n}] = \sigma\kappa, \tag{13}$$

$$[\mathbf{t} \cdot \mathbf{T} \cdot \mathbf{n}] = 0, \tag{14}$$

$$[\mathbf{u} \cdot \mathbf{n}] = 0, \tag{15}$$

$$[\mathbf{u} \cdot \mathbf{t}] = 0, \tag{16}$$

$$h_t + uh_x - w = 0, \tag{17}$$

where

$$\sigma = \frac{\sigma^*}{\rho_1^* d^2 g}.$$

We are interested in gas-liquid systems where the density and dynamic viscosity ratios are small, see Segin *et al.* [20]. Following the case of air-water (under standard conditions: $\rho_2^*/\rho_1^* = 8 \cdot 10^{-4}$, $\mu_2^*/\mu_1^* = 2 \cdot 10^{-2}$), we assume that $\bar{\rho} = \rho_2^*/\rho_1^*$ is of the order ϵ^2 and $\bar{\mu} = \mu_2^*/\mu_1^*$ is of the order ϵ, where ϵ is an aspect ratio of channel thickness to a characteristic channel length, i.e. $\bar{\rho} = \epsilon^2\rho$, $\bar{\mu} = \epsilon\mu$, and ρ, μ are $O(1)$. This distinguished limit allows us to capture the dominant physical effects in this system, while simplifying the analysis considerably.

We note that the ratio of the liquid Reynolds number to the gas Reynolds number is given by

$$\frac{Re_l}{Re_g} = \frac{d\,U_l/\nu_1^*}{d\,U_g/\nu_2^*} = \frac{\nu_2^*}{\nu_1^*}\frac{U_l}{U_g} = \frac{1}{\epsilon}\frac{U_l}{U_g},$$

where U_l is the characteristic velocity of the liquid, and U_g is the characteristic velocity of the gas. Therefore, the tangential gas velocity scale is $O(U_l/\epsilon)$ for $Re_g = Re_l = O(1)$.

Next, we assume that all changes of the flow occur on a spatial scale that is much longer than the channel thickness. Therefore, we use scaled variables $\xi = \epsilon x$ and $\zeta = z$. The kinematic boundary condition (17) then requires introducing slow time scale $\tau = \epsilon t$.

Our system of equations (8) - (11) in the long-wave limit can be written in component form as

$$\epsilon u_{\xi}^{(1)} + w_{\zeta}^{(1)} \;=\; 0, \tag{18}$$

$$\begin{aligned} &Re_l\epsilon\left[u_{\tau}^{(1)} + u^{(1)}u_{\xi}^{(1)} + \frac{1}{\epsilon}w^{(1)}u_{\zeta}^{(1)}\right] \\ &\qquad = -\epsilon p_{\xi}^{(1)} + \cos\beta \;+\; \epsilon^2\left(u_{\xi\xi}^{(1)} + \frac{1}{\epsilon^2}u_{\zeta\zeta}^{(1)}\right), \end{aligned} \tag{19}$$

$$\begin{aligned} &Re_l\epsilon\left[w_{\tau}^{(1)} + u^{(1)}w_{\xi}^{(1)} + \frac{1}{\epsilon}w^{(1)}w_{\zeta}^{(1)}\right] \\ &\qquad = -p_{\zeta}^{(1)} + \sin\beta \;+\; \epsilon^2\left(w_{\xi\xi}^{(1)} + \frac{1}{\epsilon^2}w_{\zeta\zeta}^{(1)}\right), \end{aligned} \tag{20}$$

$$\epsilon\rho_{\tau} + \epsilon\left(\rho u^{(2)}\right)_{\xi} + \left(\rho w^{(2)}\right)_{\zeta} \;=\; 0, \tag{21}$$

$$\begin{aligned} &Re_l\epsilon^2\rho\left[\epsilon u_{\tau}^{(2)} + \epsilon u^{(2)}u_{\xi}^{(2)} + w^{(2)}u_{\zeta}^{(2)}\right] \\ &\qquad = -\epsilon p_{\xi}^{(2)} + \epsilon^2\rho\cos\beta \;+\; \frac{\mu}{3}\left(4\epsilon^3 u_{\xi\xi}^{(2)} + 3\epsilon u_{\zeta\zeta}^{(2)} + \epsilon^2 w_{\zeta\xi}^{(2)}\right), \end{aligned} \tag{22}$$

$$\begin{aligned} &Re_l\epsilon^2\rho\left[\epsilon w_{\tau}^{(2)} + \epsilon u^{(2)}w_{\xi}^{(2)} + w^{(2)}w_{\zeta}^{(2)}\right] \\ &\qquad = -p_{\zeta}^{(2)} + \epsilon^2\rho\sin\beta \;+\; \frac{\mu}{3}\left(4\epsilon w_{\zeta\zeta}^{(2)} + 3\epsilon^3 w_{\xi\xi}^{(2)} + \epsilon^2 u_{\zeta\xi}^{(2)}\right). \end{aligned} \tag{23}$$

We assume a perturbation expansion for u in ϵ:

$$u^{(1)}(\xi,\zeta,\tau) = u_0^{(1)}(\xi,\zeta,\tau) + \epsilon u_1^{(1)}(\xi,\zeta,\tau) + ...,$$

and then from the continuity equation (18), it follows that

$$w^{(1)}(\xi,\zeta,\tau) = \epsilon\left\{w_0^{(1)}(\xi,\zeta,\tau) + \epsilon w_1^{(1)}(\xi,\zeta,\tau) + ...\right\}.$$

The gas velocities in the second fluid have an asymptotic expansion of the form:

$$u^{(2)}(\xi,\zeta,\tau) = \frac{1}{\epsilon}\left\{u_0^{(2)}(\xi,\zeta,\tau) + \epsilon u_1^{(2)}(\xi,\zeta,\tau) + ...\right\}.$$

From the continuity equation (21), we find appropriate expansion of w

$$w^{(2)}(\xi,\zeta,\tau) = w_0^{(2)}(\xi,\zeta,\tau) + \epsilon w_1^{(2)}(\xi,\zeta,\tau) + ...$$

In addition, we assume large surface tension (to be comparable with hydrostatic pressure and inertial effects) and define the unit-order parameter $S = \epsilon^2\sigma$. We note that we have performed a similar expansion in [20] without allowing for gas compressibility. In addition, a similar expansion was performed by Tilley *et al.* [23] without the assumption of a particular scaling of the viscosities and the densities.

From the equation of state, along with the z-component of the momentum equations, we can recover the incompressible limit if K is sufficiently large. We are interested in the case, however, when pressure gradients (equivalently density gradients) in the gas are comparable to those found in the liquid. Based on the analysis of the incompressible case [20], we know that the liquid pressure must scale as $p^{(1)} = O(1/\epsilon)$ in order for pressure gradients to drive the x-component of the fluid velocity at leading order. From the ideal gas law, a gas pressure of $O(1/\epsilon)$ results in a scaling for $K = D/\epsilon^3, D = O(1)$. This choice of scaling results in the following asymptotic expansion for the pressure in each phase:

$$p^{(i)}(\xi,\zeta,\tau) = \frac{1}{\epsilon}\left\{p_0^{(i)}(\xi,\zeta,\tau) + \epsilon p_1^{(i)}(\xi,\zeta,\tau) + ...\right\}, \qquad i = 1,2.$$

From (8) - (17), we obtain the following sequence of linear problems

$$O\left(\epsilon^{-1}\right): \qquad p_{0\zeta}^{(i)} = 0, \tag{24}$$

$$\underline{\zeta = h(\xi,\tau)}: \; p_0^{(1)} = p_0^{(2)}\ , \tag{25}$$

$$O(1): \qquad -p_{0\xi}^{(2)} + \mu u_{0\zeta\zeta}^{(2)} = 0, \tag{26}$$

$$-p_{0\xi}^{(1)} + \sin\beta + u_{0\zeta\zeta}^{(1)} = 0, \tag{27}$$

$$p_{1\zeta}^{(1)} + \cos\beta = 0, \tag{28}$$

$$p_{1\zeta}^{(2)} = 0, \tag{29}$$

$$u_{0\xi}^{(1)} + w_{0\zeta}^{(1)} = 0, \tag{30}$$

$$\left(\rho u_0^{(2)}\right)_\xi + \left(\rho w_0^{(2)}\right)_\zeta = 0, \tag{31}$$

$$\underline{\zeta = h(\xi,\tau)}: \; u_0^{(2)} = 0\ , \tag{32}$$

$$\mu u_{0\zeta}^{(2)} - u_{0\zeta}^{(1)} = 0 \ , \tag{33}$$

$$p_1^{(1)} - p_1^{(2)} = -Sh_{\xi\xi} \ , \tag{34}$$

$$w_0^{(2)} - h_\xi u_0^{(2)} = 0 \ , \tag{35}$$

$$\underline{\zeta = 0}: \quad u_0^{(1)} = 0 \ , \tag{36}$$

$$w_0^{(1)} = 0 \ , \tag{37}$$

$$\underline{\zeta = 1}: \quad u_0^{(2)} = 0 \ , \tag{38}$$

$$w_0^{(2)} = 0 \ . \tag{39}$$

From equations $O(\epsilon^{-1})$, (24) and (25), we find that

$$p_0^{(1)}(\xi,\tau) = p_0^{(2)}(\xi,\tau) = p_0(\xi,\tau).$$

The $O(1)$ $z(\zeta)$-momentum equations, (28) and (29), with condition (34) on the interface yield

$$p_1^{(1)}(\xi,\zeta,\tau) = -(\cos\beta)\zeta + P_1(\xi,\tau),$$

and

$$p_1^{(2)}(\xi,\tau) = -h(\xi,\tau)\cos\beta + P_1(\xi,\tau) + Sh_{\xi\xi}.$$

In what follows, we refer to (as of now unknown function) $P_1(\xi,\tau)$ as the pressure correction.

The $O(1)$ $x(\xi)$-momentum equations, (26), (27), continuity equations (30), (31) with boundary conditions (36) - (39), and continuity of the tangential component of the velocity and shear stress at interface (32), (33) yield

$$u_0^{(1)} = \frac{p_{0\xi} - \sin\beta}{2}\zeta^2 + \frac{2h\sin\beta - (h+1)p_{0\xi}}{2}\zeta, \tag{40}$$

$$w_0^{(1)} = -\frac{p_{0\xi\xi}}{6}\zeta^3 + \left\{-h_\xi \sin\beta + \frac{p_{0\xi\xi}}{2}(h+1) + p_{0\xi}\frac{h_\xi}{2}\right\}\frac{\zeta^2}{2}, \tag{41}$$

$$u_0^{(2)} = \frac{p_{0\xi}}{2\mu}(\zeta-1)^2 + \frac{p_{0\xi}(1-h)}{2\mu}(\zeta-1), \tag{42}$$

$$w_0^{(2)} = -\frac{(\rho p_{0\xi})_\xi}{6\rho\mu}(\zeta-1)^3 + \frac{(\rho p_{0\xi}\,[h-1])_\xi}{4\rho\mu}(\zeta-1)^2. \tag{43}$$

The details of this procedure at $O(\epsilon)$ are given in Appendices A and B. Based on this analysis, continuity of the normal velocity (15) gives the equation for the pressure gradient, while the interfacial shape is found using the kinematic boundary condition (17)

$$
\begin{aligned}
&- \left[\frac{\rho p_\xi^{(2)}(1-h)^3}{12\mu}\right]_\xi + \epsilon\left(\rho_\tau(1-h) + \frac{h(h+2)}{4}\rho h_\xi \sin\beta + \frac{h^2(1-h)}{4}\rho_\xi \sin\beta\right) \\
&+ \epsilon\left\{\frac{h^2(h+3)}{12}\rho_\xi p_\xi - \frac{(1+h)^2}{4(1-h)}\rho h_\xi p_\xi + Re_l T\right\} = 0, \qquad (44)\\
&h_\tau + A_1 + \epsilon\left(S\frac{h^3}{3}h_{\xi\xi\xi} - \frac{h^3}{3}h_\xi\cos\beta + A_2 + Re_l I\right)_\xi = 0, \qquad (45)\\
&p^{(2)} = D\rho. \qquad (46)
\end{aligned}
$$

where

$$
\begin{aligned}
A_1 &= h^2 h_\xi \sin\beta - \left[\frac{h^2(h+3)}{12}p_\xi^{(2)}\right]_\xi,\\
A_2 &= \frac{\mu h^3 p_\xi}{4(1-h)} - \frac{\mu h^4}{4(1-h)}\sin\beta,\\
I &= \frac{h^4(7h+25)}{240}p_{\xi\tau} + \frac{13}{480}h^2(1-h)^4\frac{\rho}{\mu^2}p_\xi\left\{-h_\xi p_\xi + \frac{\rho_\xi}{\rho}p_\xi(1-h)\right\}\\
&- \frac{h^5(10h^2+7h+77)}{3360(1-h)}h_\xi p_\xi^2 + \frac{2}{15}h^6 h_\xi \sin^2\beta - \frac{h^5(29h^2+161h-378)}{20160}\frac{\rho_\xi}{\rho}p_\xi^2\\
&+ \sin\beta\left[\frac{h^6(109h+147)}{10080}\frac{\rho_\xi}{\rho}p_\xi + \frac{h^5(41h^2-49h-56)}{840(1-h)}p_\xi h_\xi\right],\\
T &= -\frac{17}{3360\mu^3}\left[\rho^2 p_\xi^2(1-h)^6 h_\xi - \rho\rho_\xi p_\xi^2(1-h)^7\right]_\xi.
\end{aligned}
$$

This system (44), (45) is closed using the appropriate boundary conditions. In the evolution equation (45), we require that the first and third derivatives vanish at both ends of the domain. This choice of boundary conditions is motivated by its simplicity and by the fact that we consider only the flow far from the entrance and the exit. In the density equation (44), we prescribe $\rho(0,t) = \rho_{in}$ and $\rho(1,t) = \rho_{out}$, therefore also prescribing the pressure drop ($\Delta P = D\left[\rho_{out} - \rho_{in}\right]$).

We note that the asymptotic analysis ceases to be valid when i) the leading-order term in the density equation (44) becomes comparable with the third term at order $O(\epsilon)$ and ii)

A_1 and ϵA_2 in the evolution equation (45) become comparable (since pressure gradient is proportional to $1/(1-h)^3$). This occurs when

$$\frac{1}{(1-h)^3} \sim \frac{\epsilon}{(1-h)^6} \ ,$$

i.e, when $h \sim 1 - \epsilon^{1/3}$. Therefore, we consider only smaller values of h.

From the leading-order pressure gradient/density equation (44), we find that

$$(\rho_0^2)_\xi = \frac{2C(\tau)}{(1-h)^3}$$

for the density basic state, where $C(\tau)$ is a function of time resulting from integration. It is related to gas mass flow rate $q = \int_h^1 \rho u_0^{(2)} d\zeta$ by $C(\tau) = -12\mu q$. Given the boundary conditions for ρ, we solve this equation explicitly to obtain

$$\rho_0^2(\xi) = \bar{Y}\rho_{out}^2 + (1-\bar{Y})\rho_{in}^2, \tag{47}$$

where

$$\bar{Y} = \frac{Y(\xi)}{Y(1)}, \qquad Y(\xi) = \int_0^\xi \frac{1}{(h-1)^3} d\xi'.$$

Note that this density base state is spatially dependent, even to the leading order. We discuss later the consequences of this spatial dependence on the methods that we use to approach the linear stability analysis.

At $O(\epsilon)$ from pressure gradient/density equation (44) we find that the correction to density is given by

$$\begin{aligned} \rho_1(\xi) \ &= \ -\frac{1}{\rho_0(\xi)} \int_0^\xi \left[\frac{h_0^2 \rho_0(\xi') \sin\beta}{4D(1-h_0)} + \frac{17}{3360}\frac{D}{\mu^3}(1-h_0)^4 \rho_0 \rho_{0\xi'}^3 \right] d\xi' \\ &- \ \frac{1}{\rho_0(\xi)} \int_0^\xi \frac{h_0^2(h_0+3)}{12(1-h_0)^3} \int_0^{\xi'} \rho_{0\hat{\xi}} d\hat{\xi} d\xi'. \end{aligned} \tag{48}$$

Before proceeding with the linear stability analysis of the system (44),(45), we give the resulting equations obtained if we let $\rho_\xi \to 0$ and $\rho_\tau \to 0$ and pressure be a function of spatial

coordinates (independent of density). In this limit, the this system of equations models the incompressible flow and simplifies to the following form

$$-\left[\frac{\rho p_{0\xi}(1-h)^3}{12\mu}\right]_\xi + \epsilon\left(\frac{h(h+2)}{4}\rho h_\xi \sin\beta - \left[\frac{\rho p_{1\xi}^{(2)}(1-h)^3}{12\mu}\right]_\xi\right)$$
$$+\ \epsilon\left\{-\frac{(1+h)^2}{4(1-h)}\rho h_\xi p_\xi - Re_l\frac{17}{3360\mu^3}\left[\rho^2 p_\xi^2(1-h)^6 h_\xi\right]_\xi\right\} = 0, \tag{49}$$

$$h_\tau + \hat{A}_1 + \epsilon\left(S\frac{h^3}{3}h_{\xi\xi\xi} - \frac{h^3}{3}h_\xi\cos\beta + A_2 + Re_l\hat{I}\right)_\xi = 0. \tag{50}$$

where

$$\hat{A}_1 = h^2 h_\xi \sin\beta - \left[\frac{h^2(h+3)}{12}p_{0\xi}\right]_\xi,$$
$$A_2 = \frac{\mu h^3 p_\xi}{4(1-h)} - \frac{\mu h^4}{4(1-h)}\sin\beta,$$
$$\hat{I} = \frac{h^4(7h+25)}{240}p_{\xi\tau} - \frac{13}{480}h^2(1-h)^4\frac{\rho}{\mu^2}p_\xi^2 h_\xi - \frac{h^5(10h^2+7h+77)}{3360(1-h)}h_\xi p_\xi^2$$
$$+\ \frac{2}{15}h^6 h_\xi \sin^2\beta + \sin\beta\frac{h^5(41h^2-49h-56)}{840(1-h)}p_\xi h_\xi - \left[\frac{h^2(h+3)}{12}p_{1\xi}^{(2)}\right].$$

(see also Segin *et al.* [20]). The results obtained by performing linear stability analysis of this system of equations are presented in Section III A for the purpose of establishing the direct comparison between incompressible and compressible formulations.

III. LINEAR STABILITY THEORY FOR COMPRESSIBLE TWO PHASE FLOW

In this section, we first outline the incompressible case. Then, in Section III B, we consider the compressible case $\rho_{in} = \rho_{out}$ which can be analyzed using normal-mode analysis. Section III C considers the general case that includes density difference/pressure jump across the channel. Here we typically consider a vertical channel and use μ=1, ρ_1=1, S=3, and $\epsilon = 0.01$.

A. Linear Stability Analysis for Incompressible Flow

The comparison of the incompressible flow problem to the general case provides an insight into the influence of compressibility on the interfacial dynamics. Linear stability analysis of two-layer incompressible system was considered by Charru and Fabre [6], and Tilley *et al.* [22]. We note that Tilley *et al.* [22] consider the flow with constraint of constant flow rate, while here we concentrate on flow driven by a prescribed pressure drop ΔP, which is experimentally realizable configuration. Despite this difference, the linear stability is similar in both cases and based on normal mode expansion, as outlined below. Furthermore, one can easily transform from one configuration to the other by using the relation

$$\Delta P = \frac{12\mu q}{(1-h_0)^3},$$

where h_0 is the fixed basic interfacial height (the same for constant ΔP and constant q).

The linear stability analysis is performed by applying the expansion

$$h(\xi,\tau) = h_0 + \delta_0 e^{ik(\xi - c\tau)}, \tag{51}$$

in (49) - (50) and assuming that the perturbation δ_0 is small. We obtain

$$\begin{aligned}
kc_i &= \epsilon k^2 \left[Re_l I(\Delta P) - \frac{h_0^3}{3}\cos\beta - \frac{S}{3}h_0^3 k^2 \right], \\
I(\Delta P) &= D_1(\Delta P)^2 + D_2 \Delta P + D_3, \\
D_1 &= \frac{h_0^5(5h_0^3 + 72h_0^2 + 371h_0 + 224)}{1680(1-h_0)^2} \\
&\quad + \frac{\rho}{\mu^2}\frac{h_0^2(1 - 15h_0^2 + 40h_0^3 - 35h_0^4 + 24h_0^5 + 5h_0^6)}{1680(1-h_0)^2}, \\
D_2 &= \frac{h_0^5(65h_0^2 + 623h_0 + 112)}{1680(1-h_0)}\sin\beta, \\
D_3 &= \frac{2}{15}h_0^6 \sin^2\beta.
\end{aligned} \tag{52}$$

where periodic boundary conditions are assumed. The same expression follows from Tilley *et al.* [22], if one assumes the particular scaling of densities and viscosities that is employed in this work.

If inertial effects are ignored ($Re_l = 0$), and hydrostatic effects are not destabilizing ($\cos\beta \geq 0$) the flow is always stable. Figure 2 shows the stability diagram resulting from (52) in the more interesting case, where inertial effects are present ($Re_l > 0$). Here we observe that the flow is destabilized under sufficient shear, with the stability boundaries nearly symmetric under $\Delta P \leftrightarrow -\Delta P$; this approximate symmetry is due to the fact that the dominant term in the definition of $I(\Delta P)$ (see (52)) is D_1, which is $O(h_0^2)$, while the rest of the terms is of $O(h_0^5)$, or higher. However, the slight asymmetry leads to instabilities in the limit of vanishing k and ΔP, viz. Fig. 2. Therefore, an incompressible flow without applied pressure drop is *unstable* for small wave numbers. We discuss whether this result propagates to the compressible case in the following section.

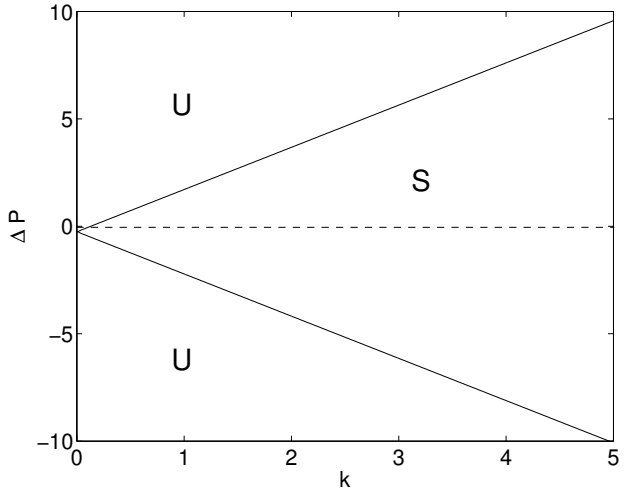

FIG. 2: Neutral stability curves for incompressible two-layer flow for h_0=0.5, μ=1, ρ_1=1, $\beta = \pi/2$, S=3, $\epsilon = 0.01$ and $Re_l = 1$. Unstable regions are denoted by a "U" and stable regions by "S".

B. Normal mode analysis for compressible case ($\rho_{in} = \rho_{out}$)

The special case $\rho_{in} = \rho_{out}$ (corresponding to $\Delta P = 0$) allows for normal mode analysis. Here we also apply periodic boundary conditions and expand

$$h(\xi, \tau) \; = \; h_0 + \delta_0 e^{ik(\xi - c\tau)},$$

$$\rho_0(\xi,\tau) \;=\; \bar{\rho}_0(\xi) + \Delta_0 e^{ik(\xi - c\tau)}.$$

where $\bar{\rho}_0(\xi) = \rho_0(\xi) + \epsilon\rho_1(\xi)$. When $\rho_{in} = \rho_{out}$, the correction to base density state vanishes and we obtain $\rho_0(\xi) = \bar{\rho}_0(\xi) = \rho_{in}$ (note that the base state gas flow has constant density, but compressible effects are present in the disturbance). After substituting these expansions into (44), (45), we arrive at the following system of characteristic equations

$$-ikc\epsilon\Delta_0 + ika_2\delta_0 + ika_4\Delta_0 + (ik)^2 a_5\Delta_0 = 0, \tag{53}$$

$$-ikc\delta_0 - (ik)^3 c\alpha\Delta_0 + b_1(ik)^2\Delta_0 + ikb_3\delta_0 + (ik)^2 b_4\delta_0 + b_5(ik)^4\delta_0 = 0, \tag{54}$$

where k is the wave number, and

$$a_2 = \epsilon\frac{h_0(h_0+2)}{4(1-h_0)}\rho_0\sin\beta, \qquad a_4 = \epsilon\frac{h_0^2}{4}\sin\beta, \qquad a_5 = -\frac{D(1-h_0)^2}{12\mu}\rho_0,$$

$$b_1 = -\frac{D}{12}h_0^2(h_0+3) + \epsilon\frac{\mu D h_0^3}{4(1-h_0)}, \qquad b_3 = h_0^2\sin\beta - \frac{\epsilon\mu}{4}\sin\beta\frac{h_0^3(4-3h_0)}{(1-h_0)^2},$$

$$b_4 = -\epsilon\frac{h_0^3}{3}\cos\beta + \frac{2\epsilon Re_l}{15}h_0^6\sin^2\beta, \qquad b_5 = \epsilon\frac{S}{3}h_0^3,$$

$$\alpha = \frac{D}{240}h_0^4(7h_0+25).$$

Thus, we obtain a system of two coupled equations (53), (54), which we solve to find kc; the growth rate is given by the imaginary part of this quantity.

For $D = 0$, the interfacial perturbation δ_0 in system (53), (54) does not depend on the density perturbation Δ_0, but Δ_0 depends on δ_0. In this limit, the gas dynamics are slaved to the interfacial dynamics, and hence the stability of the system is governed by the stability of the interfacial dynamics. In this case, the system of equations (53) - (54) simplifies to

$$-\; ikc\delta_0 + ikb_3\delta_0 + (ik)^2 b_4\delta_0 + b_5(ik)^4\delta_0 = 0, \tag{55}$$

$$-\; ikc\Delta_0 + ika_2\delta_0 + ika_4\Delta_0 = 0. \tag{56}$$

From (55), we obtain the same growth rate for the interfacial height as in the incompressible case (viz. (52) for $\Delta P = 0$; see also Segin [19])

$$kc_i = \epsilon k^2\left[-\frac{S}{3}h_0^3k^2 - \frac{h_0^3}{3}\cos\beta + \frac{2}{15}Re_l h_0^6\sin^2\beta\right]. \tag{57}$$

Here, short wavelengths are stabilized by capillarity, hydrostatic effects are stabilizing for $\beta < \pi/2$, and the flow is destabilized by inertial effects. Therefore, although not physical, we find that when $\Delta P = 0$ the limit $D = 0$ corresponds to the incompressible case characterized by passive gas response.

From (56), after division by ik, we obtain the characteristic equation for density mode. Since a_2 and a_4 in this characteristic equation are real coefficients, we note that the growth rate for the density mode (defined by the imaginary part of c) is not affected by the deviation from the interfacial profile. However, the density phase speed does depend on the basic interfacial height h_0 and the deviation from it, δ_0.

When $D \neq 0$, the density and interfacial modes are coupled. If we assume that the interface is flat ($\delta_0 = 0$), the density mode is stable, as can be verified from (53). Indeed, the density growth rate is given by

$$kc_i = -\frac{D(1-h_0)^2}{12\epsilon\mu}\rho_o k^2, \tag{58}$$

showing stability.

When the interfacial deviations are non-zero ($\delta_0 \neq 0$), we proceed with the general case defined by equations (53) - (54). First we note that, similarly to incompressible case, the flow characterized by $Re_l = 0$ is always stable. Therefore we concentrate on more involved $Re_l > 0$ case, and solve (53) - (54) numerically.

Figure 3 presents the resulting growth rates for the interfacial and density modes. In Fig. 3a, which shows interfacial growth rate (the incompressible case is calculated using equation (57)), we see that compressibility effects *stabilize* the flow. In particular, for small k's shown in Fig. 3, the stability changes from unstable for $D = 0$ (see Fig. 2), to stable for $D > 0$. Furthermore, this stabilizing effect is stronger for larger D's. Figure 3b shows the density mode, which is also always stable.

Therefore, if $\rho_{in} = \rho_{out}$, corresponding to $\Delta P = 0$, we see *stabilizing* effect of compressibility. Next, we proceed with examining the influence of compressibility on a two-fluid flow in the general case where $\rho_{out} \neq \rho_{in}$.

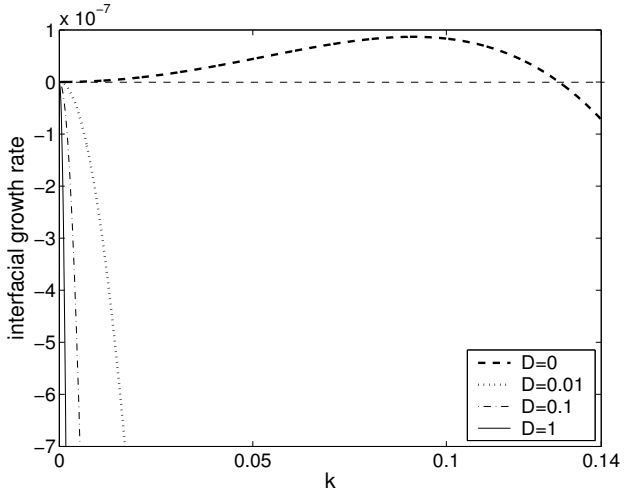

(a)

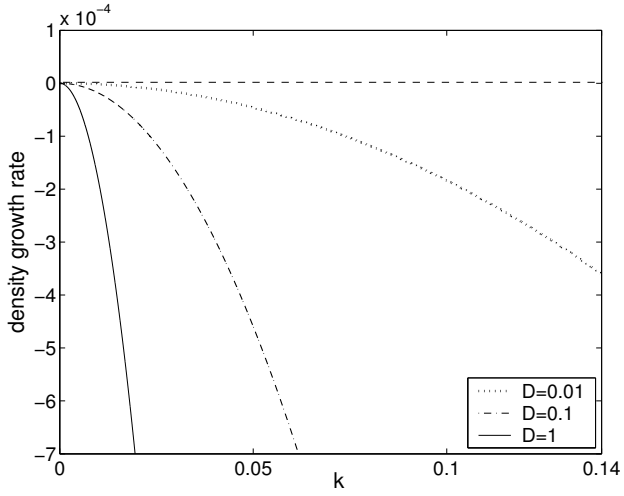

(b)

FIG. 3: Growth rate curves for (a) interfacial mode and (b) density mode vs wave number for $\rho_{out} = 1$, $h_0 = 0.5$, $Re_l = 1$ and for different values of D.

C. Linear stability for a general case ($\rho_{out} > \rho_{in}$)

If we relax the assumption of equal values of densities at the ends of the domain, we need to approach the stability problem more generally. In particular, periodic boundary

conditions used in normal mode analysis are not appropriate, so now we concentrate on the channel of fixed length. In order to test our approach to this problem, we first apply it to $\rho_{in} = \rho_{out}$ case. Therefore, we consider an interval of length 2π and perturb the interfacial height and density

$$h(\xi,\tau) \;=\; h_0 + \delta(\xi)e^{\sigma\tau}, \tag{59}$$

$$\rho_0(\xi,\tau) \;=\; \bar{\rho}_0(\xi) + \Delta(\xi)e^{\sigma\tau}, \tag{60}$$

where $\delta(\xi)$, $\Delta(\xi) \ll \epsilon$, $\bar{\rho}_0(\xi) = \rho_0(\xi) + \epsilon\rho_1(\xi)$. The base density state can be found from (47) and correction to it from (48) using $h(\xi,\tau) = h_0$

$$\rho_0^2(\xi) \;=\; \xi\rho_{out}^2 + (1-\xi)\rho_{in}^2, \tag{61}$$

$$\begin{aligned}\rho_1(\xi) \;=\;& -\frac{h_0^2\sin\beta}{6D\rho_0(\xi)(1-h_0)}\frac{\left[\{(\rho_{out}^2-\rho_{in}^2)\xi+\rho_{in}^2\}^{\frac{3}{2}}-\rho_{in}^3\right]}{\rho_{out}^2-\rho_{in}^2}\\ &-\frac{17}{26880}\frac{D(1-h_0)^4}{\mu^3\rho_0(\xi)}(\rho_{out}^2-\rho_{in}^2)^2\ln\left(1+\left\{\frac{\rho_{out}^2}{\rho_{in}^2}-1\right\}\xi\right)\\ &-\frac{h_0^2(h_0+3)(\rho_{out}^2-\rho_{in}^2)}{48\rho_0(\xi)(1-h_0)^3}\left[\left(\xi+\frac{\rho_{out}^2}{\rho_{in}^2}-1\right)\ln\left\{1+\left(\frac{\rho_{out}^2}{\rho_{in}^2}-1\right)\xi\right\}-\xi\right]\end{aligned} \tag{62}$$

By inspection, we immediately observe that ρ_1 is negligible compared to ρ_0. However, for completeness we include this correction in the analysis that follows.

After substituting the expansion (59), (60) into the linearized system of equations (44), (45) and using equations (61) and (62) we arrive at the system of characteristic equations

$$\sigma\delta + \sigma\alpha\Delta_{\xi\xi} + \bar{b}_6\Delta + \bar{b}_7\Delta_\xi + \bar{b}_1\Delta_{\xi\xi} + \bar{b}_2\delta + \bar{b}_3\delta_\xi + \bar{b}_4\delta_{\xi\xi} + b_5\delta_{\xi\xi\xi\xi} \;=\; 0, \tag{63}$$

$$\sigma\Delta + \bar{a}_1\delta + \bar{a}_2\delta_\xi + \bar{a}_6\delta_{\xi\xi} + \bar{a}_3\Delta + \bar{a}_4\Delta_\xi + \bar{a}_5\Delta_{\xi\xi} \;=\; 0. \tag{64}$$

Appendix C gives the definitions of the coefficients. We solve (63), (64) numerically using a finite difference method. This procedure leads to the system of algebraic equations

$$\mathbf{A}\cdot\mathbf{x} + \sigma\mathbf{B}\cdot\mathbf{x} = 0,$$

where A is a matrix of coefficients resulting from finite difference approximation, $\mathbf{B}$ is the matrix formed by the coefficients multiplying σ, and vector $\mathbf{x}$ is a column of unknowns $(\delta_1, ..., \delta_N, \Delta_1, ..., \Delta_N)$.

We perform the power method (Strang [21]) on the matrix **A** to find the growth rate for a given wave number. Table I shows that there is a good agreement of the growth rates obtained using the power method and the normal mode analysis at small wave numbers which are of interest here, therefore justifying usage of the power method. We note in passing that such a good agreement is not as easily obtained for higher wavenumbers since the method is more prone to numerical instabilities, due to a large condition number of the matrix **A**.

TABLE I: Growth-rate comparison between the power method and normal modes analysis. We use a grid with $N = 64$ points to approximate growth rate for the wave number k=1 and $N = 128$ for k=2.

Wave number	*Power method*	*Normal modes*
1	-2.081660	-2.081644
2	-8.3266	-8.3316

We next apply the power method to the general case, where $\rho_{in} \neq \rho_{out}$. In order to better understand the influence of compressibility of gas we first consider in Section III C 1 the system where inertial effects are ignored, and then include these effects in Section III C 2.

1. Linear stability analysis without inertial effects

For $Re_l = 0$, the system of characteristic equations (63) - (64) reduces to

$$\sigma\delta + b_1\Delta_{\xi\xi} + b_2\delta + b_3\delta_\xi + b_4\delta_{\xi\xi} + b_5\delta_{\xi\xi\xi\xi} = 0, \tag{65}$$

$$\sigma\Delta + a_1\delta + a_2\delta_\xi + a_3\Delta + a_4\Delta_\xi + a_5\Delta_{\xi\xi} = 0. \tag{66}$$

where the definitions of the a_i's and b_i's are given in Appendix C.

Figure 4 presents the dependence of the maximum growth rate on the parameter D for few different cases. We note that $D = 0$ corresponds to the incompressible limit, which is

always stable for $Re_l = 0$. Nonzero D's may, however, lead to instability. Therefore, these results imply that compressibility may *destabilize* the flow.

Figure 4 shows that instability develops as either ρ_{out} or h_0 are increased. For example, if we fix $\rho_{out} = 2$, we see that an increase of h_0 modifies the dynamics of the flow drastically as D is increased: from stable flow (h_0=0.1) to unstable ($h_0 = 0.5$). Here, we expect that the observed behavior of the maximum growth rate results from the competition between advection (due to the significant value of the induced driving force) and capillarity. At the cutoff value of D (≈ 3.7 for $\rho_{out} = 2$ and $h_0 = 0.5$), these two mechanisms balance each other. When we fix $h_0 = 0.5$, and change ρ_{out} from 2 (solid line) to 5 (dashed line), we observe that instabilities develop at smaller value of D for larger ρ_{out}. We note in passing that the growth rates shown in Fig. 4 are much larger in absolute value compared to the growth rates in the case $\rho_{in} = \rho_{out}$ shown in Fig. 3; this illustrates the fact that for our choice of parameters, the stability of the interface is predominantly determined by the imposed gas flow.

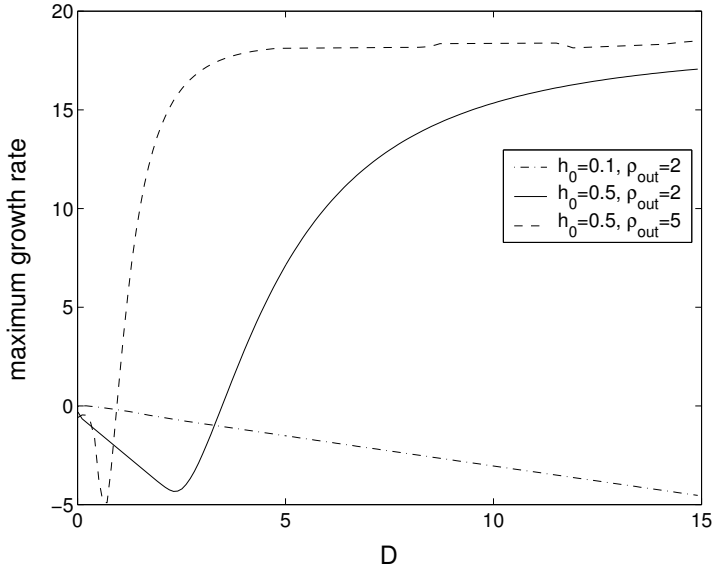

FIG. 4: Dependence of the maximum growth rate on D for $Re_l = 0$.

2. Linear stability analysis including inertial effects

We proceed with the inclusion of inertial effects. Note that in single phase liquid films the liquid inertia is the source of linear instability in the long-wave régime (Benjamin [3], Yih [25]).

Figure 5a shows the maximum growth rates vs. h_0 for four different combinations of ρ_{out} and D. The main features of the results are as follows: (i) For sufficiently small h_0, the flow is stable; (ii) This region of h_0 that corresponds to stability is decreased as ρ_{out} and/or D are increased.

Although these results are consistent with the ones presented in the previous sections, some features require more careful explanation. In particular, the presence of sharp 'corners' for $\rho_{out} = 5$, $D = 5$, close to $h_0 = 0.23$ may appear surprising. More details of this particular case are presented in Fig. 5b. We see that multiple unstable modes are present. Therefore, one 'jumps' from one unstable mode to another as one follows the most unstable mode through $h_0 = 0.23$. Figure 6, which shows the spatial eigenfunction profiles that correspond to the maximum growth rate/eigenvalue in the vicinity of $h_0 = 0.23$, confirms this observation. The change of the eigenfunctions as h_0 is increased shows that we switch to a different eigenvalue close to $h_0 = 0.23$ as h_0 increases.

Next, we consider parametric plots obtained using a fixed parameter D, with the goal of understanding in more detail the influence of liquid inertia on the stability. Figure 7 shows neutral stability curves that separate the parameter space in stable (below the curves) and unstable (above the curves) regions. The main features of the results shown in this figure are as follows:

- Compressibility may lead to instability in the flow characterized by $Re_l = 0$, which is always stable in the incompressible limit. Larger D's lead to a wider range of the parameter space $[h_0, \rho_{out}]$ where the flow is unstable. However, rather strong driving $\rho_{out} \gg \rho_{in}$ is needed for this instability to occur.

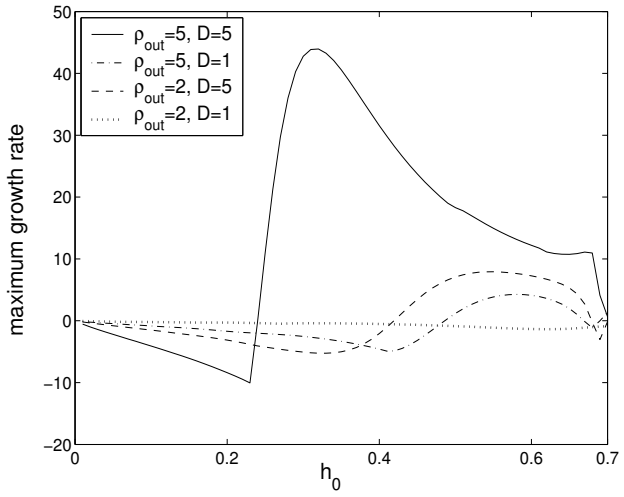

(a)

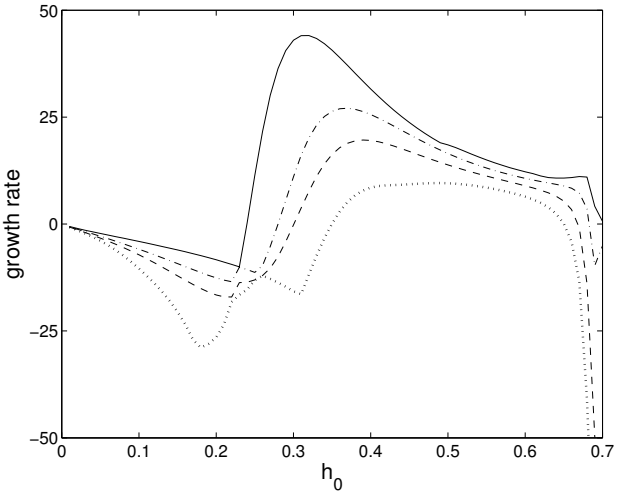

(b)

FIG. 5: (a) The growth rate of the most unstable mode vs. interfacial height for $Re_l = 1$. Sharp corner in the growth rate for $\rho_{out} = 5$, $D = 5$ correspond to the crossing eigenvalues. (b) The growth rates of unstable modes for $\rho_{out} = 5$, $D = 5$. The solid curve outlines the most unstable mode for a given h_0.

- Similar to the incompressible limit, inertial effects destabilize the flow. Figure 7 shows that this effect is particularly relevant for small h_0's.

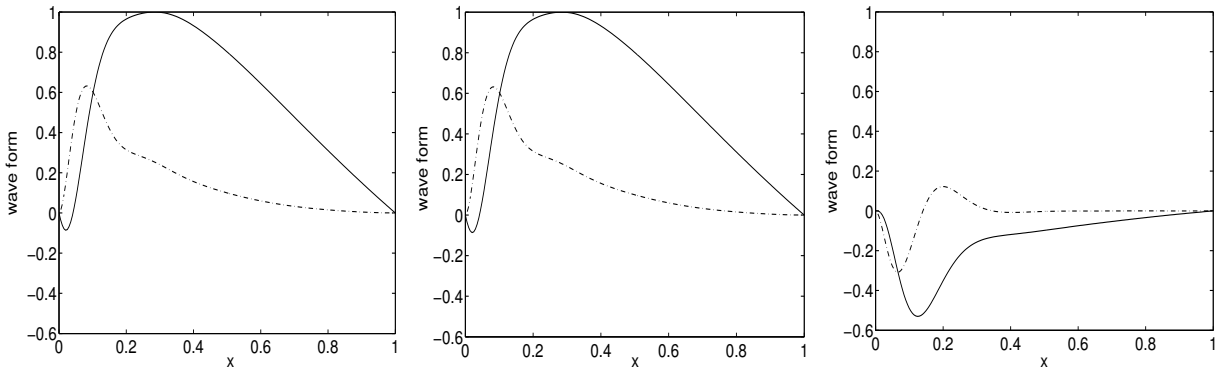

(a) $h_0 = 0.2301$ (b) $h_0 = 0.2302$ (c) $h_0 = 0.2303$

FIG. 6: Dependence of the form of the eigenfunction on the basic interfacial height for $Re_l = 1$, $D = 5$, $\rho_{out} = 5$. The interfacial mode is plotted as a dash-dotted line and density mode as a solid line. The change in the shape of the eigenfunction corresponds to crossing eigenvalues and explains the sharp corner in the maximum growth rate plot shown in Fig. 5.

We compare the stability properties between incompressible and compressible case for $Re_l > 0$. Since physical experiments typically control the pressure drop, and not the density, we replot the results from the Fig. 7 for $Re_l = 1$ in the $[h_0, \Delta P]$ space. This plot will in addition allow us to directly discuss the effect of compressibility on the stability of the flow, since ΔP is a well defined quantity in the incompressible limit as well.

Figure 8 shows the neutral stability curves in $[h_0, \Delta P]$ space, including incompressible limit. Similarly to the results obtained for $\Delta P = 0$ (i.e., $\rho_{in} = \rho_{out}$, see Fig. 3) we find *stabilizing* effect of compressibility, in particular for small values of h_0.

One may wonder why is the influence of compressibility different in the flows with and without inertial effects. One interpretation of this result is that, under the assumptions used in this work, the influence of driving by imposed pressure drop in the incompressible limit is

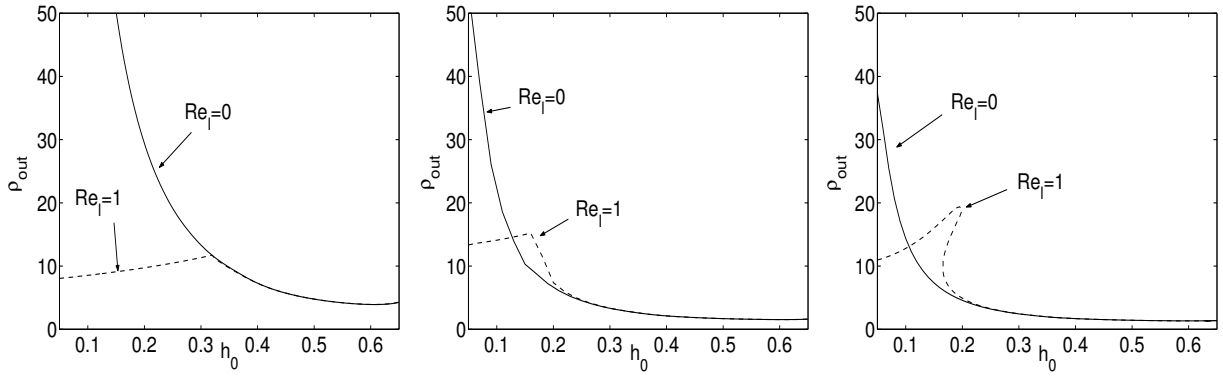

(a) D=1. (b) D=5. (c) D=8.

FIG. 7: Graphs of neutral stability curves for $Re_l = 0$ and $Re_l = 1$ for different values of D. The flow is stable below the neutral stability curves and unstable above them.

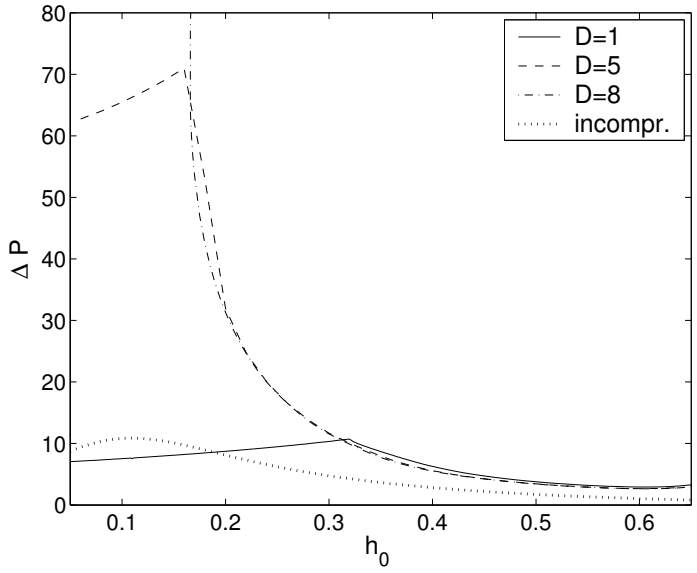

FIG. 8: Neutral stability curves in $\Delta P - h_0$ plane for $Re_l = 1$. The flow is stable below the neutral stability curves and unstable above them.

tied to the inertial response, see (52). Therefore, there is no influence of imposed pressure drop and resulting shear stresses if $Re_l = 0$. More general treatment that allows for the gas to compress relaxes this link between inertial effects and imposed shear, leading to instability

for sufficiently strong shear. However, if inertial effects are included in consideration, then the interface may become more stable under full compressible treatment, since the effect of imposed shear may be absorbed by the density modes, which is not the case under incompressible limit. This result is consistent with the works considering weakly compressible flow, cited in the Introduction.

IV. CONCLUSIONS

We have investigated the nonlinear evolution of the interface between two immiscible fluids in an inclined channel. Motivated by air-water systems, we employ a particular scaling of gas/liquid viscosities and densities. This scaling allows us to formulate a tractable problem, in which various effects, such as liquid inertia, or gas compressibility, can be clearly understood.

Following this scaling, through a lubrication approximation we derive a system of nonlinear evolution equation that governs the motion of the interface between the two fluids and the gas pressure. The lubrication approach includes the inertial effects of the liquid layer and the Reynolds stress terms in the gas. Although performing linear stability analysis for the compressible case is complicated by the fact that the base density state is spatially dependent, we are able to solve the resulting problem numerically and extract the influence of compressibility on the stability properties of the flow.

There are several overall conclusions of this work. In the case of vanishing imposed pressure drop ($\Delta P = 0$), we find that compressibility removes long wavelength instability that is present in the incompressible flow for $Re_l > 0$. Still for $\Delta P = 0$, and for $Re_l = 0$, the flow is stable both with and without compressibility. For the flows where $\Delta P > 0$, we find that compressibility has more involved effects. Here, the flows characterized by $Re_l = 0$ may be destabilized by compressibility effects, in particular for strong driving (i.e., large $\rho_{out} - \rho_{in}$, or large ΔP). This is due to the fact that in incompressible case, the effect of

ΔP on stability is present only for nonzero Re_l, while this is not the case if compressibility effects are included. However, if $Re_l > 0$, compressibility typically stabilizes the interface, i.e., it increases the region of the parameter space $[h_0, \rho_{out} - \rho_{in}]$ which the flow is stable.

An interesting artifact of the presented results corresponds to the spatial behavior of the density and interfacial disturbances (see Fig. 6). Interfacial deflections are localized near the inlet. One argument for the onset of flooding is the presence of a localized disturbance near the inlet prior to the event. These results suggest that a linear theory with the appropriate boundary conditions on the density and interfacial height at the liquid inlet and outlet may provide the criteria for the flooding event. This work focuses on one possible set of boundary conditions, but a matched asymptotic expansion local to the channel ends is needed to see if this approach describes the flooding event. Future work will concentrate on this and other issues relevant to numerous applications of two-fluid flows.

APPENDIX A: DERIVATION OF THE EVOLUTION EQUATION

At $O(\epsilon)$, the $x(\xi)$-momentum and continuity equations (8) - (11) yield

$$Re_l \left[u_{0\tau}^{(1)} + u_0^{(1)} u_{0\xi}^{(1)} + u_{0\zeta}^{(1)} w_0^{(1)}\right] = -p_{1\xi}^{(1)} + u_{1\zeta\zeta}^{(1)}, \tag{A1}$$

$$Re_l \rho \left(u_0^{(2)} u_{0\xi}^{(2)} + u_{0\zeta}^{(2)} w_0^{(2)}\right) = -p_{1\xi}^{(2)} + \mu u_{1\zeta\zeta}^{(2)}, \tag{A2}$$

$$u_{1\xi}^{(1)} + w_{1\zeta}^{(1)} = 0, \tag{A3}$$

$$\rho_\tau + \left(\rho u_1^{(2)}\right)_\xi + \left(\rho w_1^{(2)}\right)_\zeta = 0, \tag{A4}$$

$$u_1^{(1)} = 0 \qquad (\zeta = 0), \tag{A5}$$

$$u_1^{(2)} = 0 \qquad (\zeta = 1), \tag{A6}$$

$$w_1^{(1)} = 0 \qquad (\zeta = 0), \tag{A7}$$

$$w_1^{(2)} = 0 \qquad (\zeta = 1), \tag{A8}$$

$$\mu u_{1\zeta}^{(2)} - u_{1\zeta}^{(1)} = 0 \qquad (\zeta = h(\xi, \tau)), \tag{A9}$$

$$w_1^{(2)} - h_\xi u_1^{(2)} - w_0^{(1)} + h_\xi u_0^{(1)} = 0 \qquad (\zeta = h(\xi, \tau)). \tag{A10}$$

Using equations (A1) - (A4) and the boundary and interfacial conditions (A5) - (A9), similarly to the analysis at the previous order, we arrive at the solution for $u_1^{(i)}$

$$u_1^{(1)} = P_{1\xi}\frac{\zeta^2}{2} + \phi\zeta + F^{(1)}(\xi,\zeta,\tau), \tag{A11}$$

$$u_1^{(2)} = \frac{P_{1\xi}+\alpha}{2\mu}(\zeta-1)^2 + \psi(\zeta-1) + F^{(2)}(\xi,\zeta,\tau), \tag{A12}$$

where

$$\begin{aligned}\phi &= \mu F_\zeta^{(2)}(\xi,h,\tau) - F_\zeta^{(1)}(\xi,h,\tau) - \frac{\mu}{h-1}F^{(2)}(\xi,h,\tau) \\ &+ \frac{\mu h}{2(h-1)}\left\{h\sin\beta - p_{0\xi}\right\} + \alpha\frac{h-1}{2} - P_{1\xi}\frac{h+1}{2},\end{aligned} \tag{A13}$$

$$\psi = \frac{F^{(2)}(\xi,h,\tau)}{1-h} + \frac{(P_{1\xi}+\alpha)(1-h)}{2\mu} + \frac{h\left(h\sin\beta - p_{0\xi}\right)}{2(h-1)}, \tag{A14}$$

$$\alpha = Sh_{\xi\xi\xi} - h_\xi\cos\beta. \tag{A15}$$

We refer to the Appendix B for the definition of the inertial terms $F^{(i)}$.

APPENDIX B: DERIVATION OF THE INERTIAL TERMS $F^{(i)}(\xi,\zeta,\tau)$ FOR COMPRESSIBLE CASE

To find the inertial term $F^{(2)}(\xi,\zeta,\tau)$ in (A11) and (A12), we need to solve the problem:

$$F_{\zeta\zeta}^{(2)}(\xi,\zeta,\tau) = Re_l\frac{\rho}{\mu}\left(u_0^{(2)}u_{0\xi}^{(2)} + u_{0\zeta}^{(2)}w_0^{(2)}\right), \tag{B1}$$

$$F^{(2)}(\xi,1,\tau) = 0, \tag{B2}$$

$$F_\zeta^{(2)}(\xi,1,\tau) = 0. \tag{B3}$$

After integrating (B1) and, using the boundary conditions (B2), (B3), we obtain:

$$\begin{aligned}F^{(2)}(\xi,\zeta,\tau) &= a_1^{(2)}(\zeta-1)^6 + a_2^{(2)}(\zeta-1)^5 + a_3^{(2)}(\zeta-1)^4, \\ a_1^{(2)} &= Re_l\ \frac{\rho p_{0\xi}}{120\mu^3}\left(\frac{h_\xi p_{0\xi}}{1-h} - \frac{\rho_\xi}{\rho}p_{0\xi}\right), \\ a_2^{(2)} &= Re_l\frac{\rho p_{0\xi}}{80\mu^3}(1-h)\left(\frac{h_\xi p_{0\xi}}{1-h} - \frac{\rho_\xi}{\rho}p_{0\xi}\right), \\ a_3^{(2)} &= Re_l\frac{\rho p_{0\xi}}{48\mu^3}(1-h)^2\left(\frac{h_\xi p_{0\xi}}{1-h} - \frac{\rho_\xi}{\rho}p_{0\xi}\right).\end{aligned}$$

Similarly for $F^{(1)}(\xi,\zeta,\tau)$ we have:

$$F^{(1)}_{\zeta\zeta}(\xi,\zeta,\tau) = Re_l\left[u^{(1)}_{0\tau} + u^{(1)}_0 u^{(1)}_{0\xi} + u^{(1)}_{0\zeta} w^{(1)}_0\right], \tag{B4}$$

with the following boundary conditions:

$$F^{(1)}(\xi,0,\tau) \;=\; 0, \tag{B5}$$

$$F^{(1)}_{\zeta}(\xi,0,\tau) \;=\; 0. \tag{B6}$$

After integrating (B4) and applying the boundary conditions (B5), (B6):

$$F^{(1)}(\xi,\zeta,\tau) = a^{(1)}_1\zeta^6 + a^{(1)}_2\zeta^5 + a^{(1)}_3\zeta^4 + a^{(1)}_4\zeta^3, \tag{B7}$$

where

$$\begin{aligned}
a^{(1)}_1 &= Re_l\frac{p_{0\xi\xi}}{360}\left(p_{0\xi} - \sin\beta\right),\\
a^{(1)}_2 &= Re_l\frac{p_{0\xi\xi}}{60}\left\{h\sin\beta - \frac{p_{0\xi}}{2}(h+1)\right\},\\
a^{(1)}_3 &= Re_l\frac{1}{24}\left\{p_{0\xi\tau} + \left[h\sin\beta - \frac{p_{0\xi}}{2}(h+1)\right]\left[h_\xi\sin\beta - \frac{p_{0\xi\xi}}{2}(h+1) - \frac{p_{0\xi}h_\xi}{2}\right]\right\},\\
a^{(1)}_4 &= Re_l\frac{2h_\tau\sin\beta - p_{0\xi\tau}(h+1) - h_\tau p_{0\xi}}{12}.
\end{aligned}$$

APPENDIX C: DEFINITION OF THE COEFFICIENTS IN THE SYSTEM OF CHARACTERISTIC EQUATIONS

The coefficients entering the system of characteristic equations (63) - (64) are as follows

$$\bar{b}_1 = b_1 + \epsilon Re_l\theta_6, \quad \bar{b}_2 = b_2 + \epsilon Re_l\theta_1, \quad \bar{b}_3 = b_3 + \epsilon Re_l\theta_2,$$

$$\bar{b}_4 = b_4 + \epsilon Re_l\theta_3, \quad \bar{b}_6 = \epsilon Re_l\theta_4, \quad \bar{b}_7 = \epsilon Re_l\theta_5,$$

$$\bar{a}_1 = a_1 + Re_l\gamma_3, \quad \bar{a}_2 = a_2 + Re_l\gamma_1, \quad \bar{a}_3 = a_3 + Re_l\gamma_4,$$

$$\bar{a}_4 = a_4 + Re_l\gamma_5, \quad \bar{a}_5 = a_5 + Re_l\gamma_6, \quad \bar{a}_6 = Re_l\gamma_2, \quad \alpha = \frac{D}{240}h_0^4(7h_0+25),$$

with

$$
\begin{aligned}
a_1 &= \frac{D}{12}\frac{-h_0^2+2h_0+3}{(1-h_0)^2}\left(\rho_{0\xi}^2+2\epsilon\rho_{0\xi}\rho_{1\xi}\right)+\frac{D(1-h_0)}{6\epsilon\mu}\left[\rho_{0\xi}^2+\rho_0\rho_{0\xi\xi}+\epsilon(\rho_0\rho_1)_{\xi\xi}\right],\\
a_2 &= -\frac{D}{4}\left(\frac{1+h_0}{1-h_0}\right)^2(\rho_0\rho_{0\xi}+\epsilon(\rho_0\rho_1)_\xi)+\frac{h_0(h_0+2)}{4(1-h_0)}(\rho_0+\epsilon\rho_1)\sin\beta\\
&\quad+\frac{D}{4\epsilon\mu}(1-h_0)\left(\rho_0\rho_{0\xi}+\epsilon(\rho_0\rho_1)_\xi\right),\\
a_3 &= -\frac{D}{12\epsilon\mu}(1-h_0)^2\left(\rho_{0\xi\xi}+\epsilon\rho_{1\xi\xi}\right),\\
a_4 &= \frac{h_0^2}{4}\sin\beta+\frac{D}{6}\frac{h_0^2(h_0+3)}{1-h_0}\left(\rho_{0\xi}+\epsilon\rho_{1\xi}\right)-\frac{D(1-h_0)^2}{6\epsilon\mu}\left(\rho_{0\xi}+\epsilon\rho_{1\xi}\right),\\
a_5 &= -\frac{D(1-h_0)^2}{12\epsilon\mu}\left(\rho_0+\epsilon\rho_1\right),\qquad b_1=-\frac{D}{12}h_0^2(h_0+3)+\epsilon\frac{\mu D h_0^3}{4(1-h_0)},\\
b_2 &= \frac{D}{4}h_0(h_0+2)\left(\rho_{0\xi\xi}+\epsilon\rho_{1\xi\xi}\right)+\frac{\epsilon\mu D}{4}\left[\frac{h_0^3\rho_{0\xi\xi}}{(1-h_0)^2}+\frac{3h_0^2}{1-h_0}\rho_{0\xi\xi}\right],\\
b_3 &= h_0^2\sin\beta-\frac{D}{4}h_0(h_0+2)\left(\rho_{0\xi}+\epsilon\rho_{1\xi}\right)-\frac{\epsilon\mu}{4}\sin\beta\frac{h_0^3(4-3h_0)}{(1-h_0)^2}\\
&\quad+\frac{\epsilon\mu D}{4}\frac{h_0^2(3-2h_0)}{(1-h_0)^2}\rho_{0\xi},\\
b_4 &= -\epsilon\frac{h_0^3}{3}\cos\beta,\qquad b_5=\epsilon\frac{S}{3}h_0^3,
\end{aligned}
$$

and

$$
\begin{aligned}
\theta_1 &= -\frac{D^2}{20160}\left[\frac{3\rho_{0\xi}^2\rho_{0\xi\xi}}{\rho_0}-\frac{\rho_{0\xi}^4}{\rho_0^2}\right]h_0^4(203h_0^2+966h_0-1890)\\
&\quad+\frac{13}{240}\frac{D^2}{\mu^2}\rho_0\rho_{0\xi}\rho_{0\xi\xi}h_0(2-7h_0)(1-h_0)^4\\
&\quad+\frac{D}{10080}\sin\beta h_0^5(763h_0+882)\left[\frac{2\rho_{0\xi}\rho_{0\xi\xi}}{\rho_0}-\frac{\rho_{0\xi}^3}{\rho_0^2}\right],\\
\theta_2 &= -\frac{D^2}{1680}\frac{h_0^5(10h_0^2+7h_0+77)}{1-h_0}\rho_{0\xi}\rho_{0\xi\xi}-\frac{D^2}{20160}\frac{\rho_{0\xi}^3}{\rho_0}h_0^4(203h_0^2+966h_0-1890)\\
&\quad-\frac{13}{480}\frac{D^2}{\mu^2}h_0^2(1-h_0)^4\left[\rho_{0\xi}^3+2\rho_0\rho_{0\xi}\rho_{0\xi\xi}\right]+\frac{13}{480}\frac{D^2}{\mu^2}h_0(1-h_0)^4(2-7h_0)\rho_0\rho_{0\xi}^2\\
&\quad+\sin\beta\left[\frac{D}{840}\frac{h_0^5(41h_0^2-49h_0-56)}{1-h_0}\rho_{0\xi\xi}+\frac{D}{1440}\frac{\rho_{0\xi}^2}{\rho_0}h_0^5(109h_0+126)\right]\\
\theta_3 &= -\frac{D^2}{3360}\frac{h_0^5(10h_0^2+7h_0+77)}{1-h_0}\rho_{0\xi}^2+\frac{2}{15}h_0^6\sin^2\beta-\frac{13}{480}\frac{D^2}{\mu^2}\rho_0\rho_{0\xi}^2h_0^2(1-h_0)^4\\
&\quad+\frac{D}{840}\sin\beta\frac{h_0^5(41h_0^2-49h_0-56)}{1-h_0}\rho_{0\xi},
\end{aligned}
$$

$$
\begin{aligned}
\theta_4 &= -\frac{D^2}{20160}\left[\frac{2\rho_{0\xi}^4}{\rho_0^3}-\frac{3\rho_{0\xi}^2\rho_{0\xi\xi}}{\rho_0^2}\right]h_0^5(29h_0^2+161h_0-378)\\
&+ \frac{13}{240}\frac{D^2}{\mu^2}\rho_{0\xi}\rho_{0\xi\xi}h_0^2(1-h_0)^5+\frac{D}{5040}\sin\beta h_0^6(109h_0+147)\left[\frac{\rho_{0\xi}^3}{\rho_0^3}-\frac{\rho_{0\xi}\rho_{0\xi\xi}}{\rho_0^2}\right],\\
\theta_5 &= -\frac{D^2}{10080}\left[\frac{3\rho_{0\xi}\rho_{0\xi\xi}}{\rho_0}-\frac{2\rho_{0\xi}}{\rho_0}\right]h_0^5(29h_0^2+161h_0-378)\\
&+ \frac{13}{240}\frac{D^2}{\mu^2}\rho_0\rho_{0\xi\xi}h_0^2(1-h_0)^5+\frac{D}{10080}\sin\beta h_0^6(109h_0+147)\left[\frac{2\rho_{0\xi\xi}}{\rho_0}-\frac{3\rho_{0\xi}^2}{\rho_0^2}\right],\\
\theta_6 &= -\frac{D^2}{6720}\frac{\rho_{0\xi}^2}{\rho_0}h_0^5(29h_0^2+161h_0-378)+\frac{13}{240}\frac{D^2}{\mu^2}\rho_0\rho_{0\xi}h_0^2(1-h_0)^5\\
&+ \frac{D}{5040}\sin\beta h_0^6(109h_0+147)\frac{\rho_{0\xi}}{\rho_0},
\end{aligned}
$$

and

$$
\begin{aligned}
\gamma_1 &= -\frac{51}{1120\mu^3}(1-h_0)^5\left(\rho_0\rho_{0\xi}^3+\epsilon\left[\rho_1\rho_{0\xi}^3+3\rho_0\rho_{0\xi}^2\rho_{1\xi}\right]\right)\\
&\quad -\frac{17}{1680\mu^3}(1-h_0)^5\left(\rho_0^2\rho_{0\xi}\rho_{0\xi\xi}+\epsilon\rho_0\left[\rho_0\rho_{0\xi\xi}\rho_{1\xi}+\rho_0\rho_{0\xi}\rho_{1\xi\xi}-2\rho_{0\xi}\rho_{0\xi\xi}\rho_1\right]\right),\\
\gamma_2 &= -\frac{17}{3360\mu^3}\left(\rho_0^2\rho_{0\xi}^2+2\epsilon\rho_0\rho_{0\xi}^2(\rho_0\rho_1)_\xi\right)(1-h_0)^5,\\
\gamma_3 &= \frac{17}{560\mu^3}\left(\rho_{0\xi}^4+4\epsilon\rho_{0\xi}^3\rho_{1\xi}\right)(1-h_0)^5\\
&\quad -\frac{51}{560\mu^3}(1-h_0)^5\left(\rho_0\rho_{0\xi}^2\rho_{0\xi\xi}+\epsilon\rho_{0\xi}\left[2\rho_0\rho_{0\xi\xi}\rho_{1\xi}+\rho_{0\xi}\rho_{0\xi\xi}\rho_1+\rho_0\rho_{0\xi}\rho_{1\xi\xi}\right]\right),\\
\gamma_4 &= \frac{17}{1120\mu^3}\left(\rho_{0\xi}^2\rho_{0\xi\xi}+\epsilon\rho_{0\xi}\left[\rho_{0\xi}\rho_{1\xi\xi}+2\rho_{0\xi\xi}\rho_{1\xi}\right]\right)(1-h_0)^6,\\
\gamma_5 &= \frac{17}{840\mu^3}(1-h_0)^6\left(\rho_{0\xi}^3+3\epsilon\rho_{0\xi}^2\rho_{1\xi}\right)\\
&\quad +\frac{17}{560\mu^3}(1-h_0)^6\left(\rho_0\rho_{0\xi}\rho_{0\xi\xi}+\epsilon\left[\rho_0\rho_{0\xi\xi}\rho_{1\xi}+\rho_1\rho_{0\xi}\rho_{0\xi\xi}+\rho_0\rho_{0\xi}\rho_{1\xi\xi}\right]\right),\\
\gamma_6 &= \frac{17}{1120\mu^3}(1-h_0)^6\left(\rho_0\rho_{0\xi}^2+\epsilon\rho_{0\xi}\left[2\rho_0\rho_{1\xi}+\rho_{0\xi}\rho_1\right]\right).
\end{aligned}
$$

---

[1] A. Alexakis, Y. Young, and R. Rosner. Shear stability of fluid interfaces: Stability analysis. *Phys. Rev. Lett. E*, 65:026313, 1–17, 2002.

[2] S. G. Bankoff and S. C. Lee. *Multiphase science and technology. A critical review of the flooding literature.* Hewitt G. F., Delhaye J. M., Zuber N., Hemisphere, 1986.

[3] T. B. Benjamin. Wave formation in laminar flow down an inclined plane. *J. Fluid Mech.*, 2:554–574, 1957.

[4] W. S. Bousman, J. B. McQuillen, and L. C. Witte. Gas-liquid flow patterns in microgravity: effects of tube diameter, liquid viscosity and surface tension. *Int. J. Multiphase Flow*, 22:1035–1053, 1996.

[5] H.-C. Chang. Nonlinear waves on liquid film surfaces. Part I: Flooding in a vertical tube. *Chemical Engineering Science*, 41:2463–2476, 1986.

[6] F. Charru and Fabre J. Long waves at the interface between two viscous fluids. *Phys. Fluids*, 6:1223–1235, 1994.

[7] A. E. Dukler, J. A. Fabre, J. B. McQuillen, and R. Vernon. Gas liquid flow at microgravity conditions: flow patterns and their transitions. *Int. J. Multiphase Flow*, 14:389–400, 1988.

[8] T. E. Faber. *Fluid Dynamics For Physicists*. Cambridge University Press, Cambridge, 2001.

[9] A. C. Fowler and P. E. Lisseter. Flooding and flow reversal in annular two-phase flows. *SIAM J. Appl. Math.*, 52:15–33, 1992.

[10] T. Hagstrom and J. Lorenz. All-time existence of classical solutions for slightly compressible flows. *SIAM J. Math. Anal.*, 29:652–672, 1998.

[11] J. Kirshberg, K. Yerkes, and D. Liepmann. Demonstration of a micro-cpl based on mems fabrication technologies. In *Proceedings from the 35th Intersociety Energy Conversion Engineering Conference, Vol. 2*, pages 1198–1204. 2000.

[12] D. Livescu. Compressibility effects on the Rayleigh-Taylor instability growth between immiscible fluids. *Phys. Fluids*, 16:118–127, 2004.

[13] A. A. Mouza, S. V. Paras, and A. J. Karabelas. Incipient flooding in inclined tubes of small diameter. *Int. J. Multiphase Flow*, 29:1395–1412, 2003.

[14] I. Mudawar. Assessment of high-heat thermal management schemes. *IEEE Trans. Comp. Pack. Tech.*, 24:122–141, 2001.

[15] G. Odddie and A. J. R. Pearson. Flow-rate measurement in two-phase flow. *Annu. Rev. Fluid Mech.*, 36:149–172, 2004.

[16] K. Pettigrew, J. Kirshberg, K. Yerkes, D. Trebotich, and D. Liepmann. Performance of a mems based micro capillary pumped loop for chip-level temperature control. In *14th IEEE International Conference on Micro Electro Mechanical Systems*, pages 427–430. 2001.

[17] W Qu and I. Mudawar. Thermal design methodology for high=heat-flux single-phase and two-phase micro-channel heat sinks. *IEEE Trans. Comp. Pack. Tech.*, 26:598–609, 2003.

[18] Z. Rusak and J. H. Lee. On the stability of a compressible axisymmetric rotating flow in a pipe. *J. Fluid Mech.*, 501:25–42, 2004.

[19] T. Segin. *Nonlinear long-wave interfacial stability of two-layer gas-liquid flows.* PhD thesis, New Jersey Institute of Technology, 2004.

[20] T. M. Segin, B. S. Tilley, and L. Kondic. On undercompressive shocks and flooding in countercurrent two-layer flows. *J. Fluid Mech.*, 532:217–242, 2005.

[21] G. Strang. *Linear algebra and its applications.* Harcourt Brace Jovanovich College Publishers, New York, 3rd edition, 1988.

[22] B. S. Tilley, S. H. Davis, and S. G. Bankoff. Linear stability theory of two-layer fluid flow in an inclined channel. *Phys. Fluids A*, 6:3906–3922, 1994.

[23] B. S. Tilley, S. H. Davis, and S. G. Bankoff. Nonlinear long-wave stability of superposed fluids in an inclined channel. *J. Fluid Mech.*, 277:55–83, 1994.

[24] D. Trebotich, J. Kirshberg, J. Teng, and D. Liepmann. Optimization of a MEMS based micro capillary pumped loop for chip-level temperature control. In *Fourth International Conference on Modeling and Simulation in Microsystems*, pages 262–265. 2001.

[25] C.-S. Yih. Instability due to viscosity stratification. *J. Fluid Mech.*, 27:337–352, 1967.

[26] H. Zhang, I. Mudawar, and M. M. Hasan. Experimental assessment of the effects of body fore, surface tension force, and inertia on flow boiling CHF. *Int. J. Heat Mass. Transf.*, 45:4079–4095, 2002.